JACS
JOURNAL OF THE AMERICAN CHEMICAL SOCIETY
Article
pubs.acs.org/JACS

Inhibition at Perimeter Sites of Au/TiO_2 Oxidation Catalyst by Reactant Oxygen

Isabel Xiaoye Green,[†] Wenjie Tang,[‡] Monica McEntee,[†] Matthew Neurock,[†,‡] and John T. Yates, Jr.*[,†,‡]

[†]Department of Chemistry and [‡]Department of Chemical Engineering, University of Virginia, Charlottesville, Virginia 22904, United States

Supporting Information

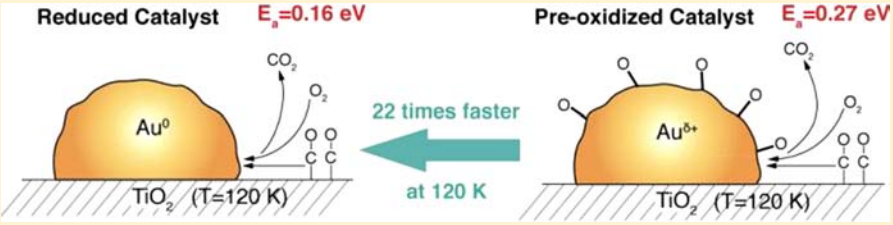

ABSTRACT: TiO_2-supported gold nanoparticles exhibit surprising catalytic activity for oxidation reactions compared to noble bulk gold which is inactive. The catalytic activity is localized at the perimeter of the Au nanoparticles where Au atoms are atomically adjacent to the TiO_2 support. At these dual-catalytic sites an oxygen molecule is efficiently activated through chemical bonding to both Au and Ti^{4+} sites. A significant inhibition by a factor of 22 in the CO oxidation reaction rate is observed at 120 K when the Au is preoxidized, caused by the oxygen-induced positive charge produced on the perimeter Au atoms. Theoretical calculations indicate that induced positive charge occurs in the Au atoms which are adjacent to chemisorbed oxygen atoms, almost doubling the activation energy for CO oxidation at the dual-catalytic sites in agreement with experiments. This is an example of self-inhibition in catalysis by a reactant species.

I. INTRODUCTION

The origin of the activity of oxide-supported nanoparticle Au catalysts has been of great interest over the last two decades.[1,2] This activity contrasts markedly with the inactivity of the bulk metal. Nanoparticle Au catalysts exhibit extraordinary efficiency and selectivity in key industrial oxidation reactions involving molecular oxygen.[3] Understanding the mechanisms by which these catalysts carry out oxidation reactions will provide valuable insights and guidance toward the design of new catalytic materials. Joining the effort of unraveling the CO oxidation process on the Au/TiO_2 catalyst lead by others,[4−8] we have shown spectroscopically that on a catalyst comprised of ∼3 nm Au particles supported on TiO_2 the catalytic activity is localized at the Au perimeter, where dual-catalytic sites involving Au atoms and Ti^{4+} ions work together at very low temperatures to activate molecular oxygen and oxidize both H_2 as well as CO.[9,10] More research is needed as many aspects of the dual-catalytic system are still unclear and under debate.

The charge state of active Au species during the catalytic reaction is one area that has been greatly debated, with different reports citing the active sites as being negative, neutral, or positively charged Au species. For instance, Au clusters deposited on oxide F centers were reported to be negatively charged and highly active for CO oxidation;[8,11−13] other experiments, however, suggest that the active sites for CO oxidation are comprised of partially oxidized (positively charged) Au centers.[14−17] In addition, there are also various reports that suggest as-synthesized cationic Au(III) is not active for CO oxidation at room temperature until reduced to metallic Au[3,18] and that the metallic Au is the active species.[18,19] Previous theoretical calculations of charge effects on Au also provided mixed conclusions as to the relationship between the Au oxidation state and the catalytic activity.[7,20−35]

Two important challenges associated with establishing the charged state of the active sites experimentally are as follows: (1) it was hard to measure the partial charge state (oxidation states between 0 and ±1) of localized Au atoms in situ directly via common techniques such as X-ray photoelectron spectroscopy, X-ray absorption near-edge structure spectroscopy, or Mössbauer spectroscopy until recently;[15,36] and (2) the reactant for the standard catalyst activity test, the CO molecule, is a strong reducing agent for Au nanoparticles at room temperature or lower.[37−39] To avoid these complications, we use the reactant CO molecule as a surface probe at very low temperatures (∼120 K) to detect the Au oxidation state during the catalytic reaction and, in addition, to kinetically track the reaction progress via in situ infrared (IR) spectroscopy. At these low temperatures reduction of cationic Au by CO does not occur during the catalytic reaction.

We previously demonstrated that at temperatures in the range 110−130 K CO molecules adsorbed on the TiO_2 support (CO/TiO_2) are the active species for CO oxidation and delivered to the dual-catalytic perimeter sites by diffusion across

Received: May 7, 2012
Published: June 27, 2012

 © 2012 American Chemical Society dx.doi.org/10.1021/ja304426b | J. Am. Chem. Soc. 2012, 134, 12717−12723

TiO_2.[9] By working at low temperatures the reaction is kinetically simplified via exclusion of higher activation energy processes. In contrast, CO adsorbed on Au sites is essentially unreactive at 120 K.[9] In the work reported here we show that preoxidation of the Au perimeter sites of the Au/TiO_2 catalyst at high temperature (473 K), to produce $Au^{\delta+}$ sites, reduced the CO oxidation activity by a factor of 22 at 120 K. The apparent activation energy for CO oxidation over the Au/TiO_2 catalyst increases from 0.16 to 0.27 eV when $Au^{\delta+}$ sites are produced by preoxidation of the catalyst. Density functional theory (DFT) calculations indicate that the origin of the local catalytic inhibition or site poisoning is conversion of Au^0 to $Au^{\delta+}$ at the Au nanoparticle perimeter that results from the strong chemisorption of oxygen atoms at these sites. Understanding the inhibition of the active Au sites in the low-temperature regime provides insight into the mechanism of the CO oxidation reaction on Au/TiO_2 catalysts at higher temperatures, thus coupling low-temperature studies to catalysis at higher temperatures.

II. EXPERIMENTAL PROCEDURES

Sample Preparation and Instrumentation. The Au/TiO_2 catalyst studied in this work was synthesized by a deposition–precipitation method reported by Zanella et al. involving $HAuCl_4{\cdot}3H_2O$, urea, and TiO_2 powder.[40] This method produces Au nanoparticles with an average diameter of ~3 nm.[40] A detailed description of the synthesis procedure can be found in the Supporting Information. A high-vacuum transmission IR cell with liquid-N_2 cooling of the samples supported on a tungsten grid was employed for the low-temperature catalytic reaction study (Figure S1, Supporting Information).[9,10]

Preoxidation of the catalyst to various stages was carried out at temperatures from 295 to 473 K in 5 Torr of O_2 for 30 min. Prereduction of the catalyst to different degrees was carried out in 0.07 Torr of CO for 5 min at temperatures in the range 120–473 K, as indicated in each experiment reported. All experiments described in this study were carried out on the same catalyst prepared by repeated oxidation in O_2 followed by reduction in CO, i.e., the catalyst was reusable for many experiments. No heating above 473 K was performed to avoid the known effect of sintering of Au nanoparticles.[6,41] Thus, a "fully-oxidized $Au^{\delta+}/TiO_2$ catalyst" and a "fully-reduced Au^0/TiO_2 catalyst" were made by O_2 oxidation or CO reduction at 473 K. Transmission electron microscope measurements of the catalyst after repeated oxidation/reduction cycles show a Au particle size distribution similar to the as-prepared catalyst (2–8 nm diameter, with a most probable diameter of 3 nm, Figure S2, Supporting Information).[9,10,40] The catalyst, oxidized and reduced at different temperatures, was cooled to 120 K in vacuum for the CO adsorption and oxidation reaction.

CO adsorption on the catalyst to saturation coverage at temperatures between 110 and 130 K was achieved by backfilling the cell with 0.07 Torr of CO gas. For the CO oxidation studies, after reaching saturation, the CO gas was evacuated from the cell for approximately 10 min to produce one monolayer (ML) coverage. An IR spectrum was taken after 8.6 min of CO evacuation in each experiment and used as the point of time zero for the reaction kinetics study. One Torr of O_2 was then introduced to the cell, and the CO oxidation reaction immediately began. FTIR spectra were taken every minute until the CO/TiO_2 adsorption feature was gone from the IR spectra (~20 min for Au^0/TiO_2 catalyst and ~60 min for $Au^{\delta+}/TiO_2$ catalyst).

Computational Methods. First-principle plane wave density functional theory (DFT) calculations carried out using the generalized gradient approximation (GGA)[42] were used herein to explore the influence of oxidized Au sites on CO oxidation. Detailed information about the calculation can be found in the Supporting Information. The Au/TiO_2 system was simulated herein by a Au nanorod supported on a rutile $TiO_2(110)$ surface. The oxide (2 × 3) unit cell has four O–Ti–O trilayers in the Z direction. The atoms in the top two trilayers of the TiO_2 slab were allowed to fully relax, while the atoms in the bottom two trilayers were fixed to their lattice positions. The 3 nm Au particle was simulated by a three-atomic-layers-high Au nanorod as shown in Figure S5, Supporting Information. All of the Au atoms were allowed to relax in the Z direction. This model has been used previously by other groups and by ourselves to find plausible reaction mechanisms and locate active sites, because the Au nanorod structure is computationally tractable and provides a sample of Au surface sites with different coordination numbers (CN).[7,9,10,28,35] However, the structure is devoid of Au corner sites, likely causing the calculations to slightly underestimate the actual catalytic reactivity.

III. RESULTS AND DISCUSSIONS

The stepwise oxidation of the catalyst was carried out to examine the Au^0 to $Au^{\delta+}$ species conversion. Figure 1a shows

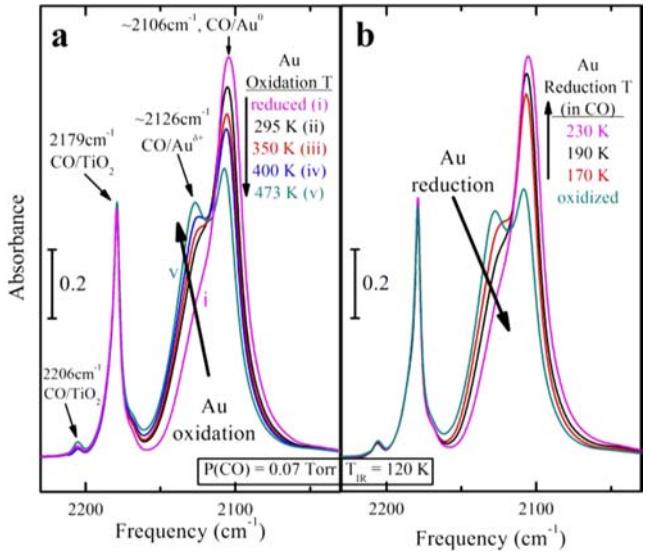

Figure 1. IR spectra of 120 K saturated CO adsorption of the Au/TiO_2 catalyst surface modification by (a) oxidation in O_2 and (b) reduction in CO at different temperatures.

the IR spectra in the CO stretching region of a reduced catalyst preoxidized to different levels. The IR absorption bands at 2179 and 2206 cm^{-1} are assigned to CO adsorbed on Ti^{4+} sites (denoted as CO/TiO_2) because identical bands are observed on a TiO_2 blank sample also held in the IR cell (Figure S3, Supporting Information). The IR band at ~2106 cm^{-1} is assigned to CO terminally adsorbed on metallic Au^0 sites based on previous investigations (denoted as CO/Au^0).[9,39,43–45] The high-frequency shoulder at ~2126 cm^{-1} is generally assigned to CO adsorbed on positively charged $Au^{\delta+}$ sites ($0 < \delta < 1$, denoted as $CO/Au^{\delta+}$).[39,44–46] As the preoxidation temperature increases from 295 to 473 K, the 2106 cm^{-1} band decreases in absorbance at saturation coverage while the 2126 cm^{-1} band increases in absorbance, indicating a transition from CO/Au^0 species to $CO/Au^{\delta+}$ species under increasingly aggressive oxidation conditions.

The Au-catalyst preoxidation process was shown to be completely reversible by observation of ν_{CO} during reduction of the oxidized $Au^{\delta+}/TiO_2$ catalyst in gas-phase CO. Figure 1b shows the 120 K–CO IR absorption spectra of the preoxidized catalyst reduced at temperatures from 170 to 230 K in 0.07 Torr of CO, where an increase of CO/Au^0 species is accompanied by a decrease of $CO/Au^{\delta+}$ species, just opposite from Figure 1a. It is noted that the Au oxidation state produced

dx.doi.org/10.1021/ja304426b | J. Am. Chem. Soc. 2012, 134, 12717–12723

by pretreatment has no influence on the neighboring CO/TiO_2 species, since the band frequency, band shape, and saturation absorbance of the CO/TiO_2 species remains unchanged upon Au oxidation/reduction. We denote the catalyst in Figure 1a(i) as the "fully-reduced Au^0/TiO_2" sample and the catalyst in Figure 1a(v) as the "fully-oxidized $Au^{\delta+}/TiO_2$" sample. The CO/Au^{1+} (ν_{CO} = 2186−2159 cm^{-1}),[38,45,47] CO/Au^{3+} ($\nu_{CO} \approx$ 2207 cm^{-1}),[47] and $CO/Au^{\delta-}$ (ν_{CO} = 2038−1900 cm^{-1})[46,48] species reported by others on Au nanoparticle catalysts using IR or other measurement techniques[11,12,14] are not found in our IR observations.

To gain quantitative knowledge of the conversion between Au^0 and $Au^{\delta+}$ species, the overlapping CO/Au^0 and $CO/Au^{\delta+}$ bands have been deconvoluted using a Lorentz function in all measurements made during the CO reduction process (part of which are presented in Figure 1b). The integrated absorbance of each deconvoluted band is used as a measurement of the amount of the corresponding species on the surface. Figure 2

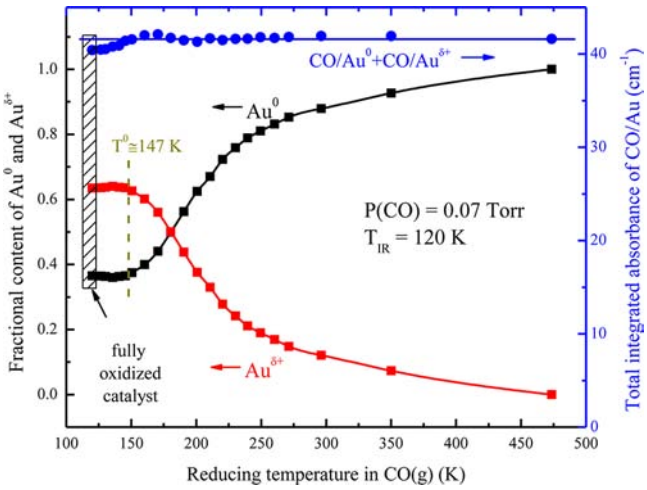

Figure 2. (Left axis) Plots of the $CO/Au^{\delta+}$ fractional conversion to CO/Au^0 species monitored by deconvolution of IR bands from Figure 1b using the Lorentz ν_{CO} line shape function and comparing the integrated absorbance of each deconvoluted band. (Right axis) Plot of the total integrated IR absorbance of $CO/Au^{\delta+}$ and CO/Au^0 species combined versus catalyst reduction temperature.

depicts conversion of $CO/Au^{\delta+}$ to CO/Au^0 as a function of increasing reduction temperature in CO. The reduction process starts above 147 K in 0.07 Torr of CO, before which little change in integrated absorbance is observed for either species. The total integrated CO absorbance on the Au^0 and $Au^{\delta+}$ sites remains constant during the reduction (Figure 2, right axis), indicating that the saturation coverage of adsorbed CO (1 ML) on the Au nanoparticles is constant for various stages of reduction, and supports the idea that the extinction coefficients of CO/Au^0 species and $CO/Au^{\delta+}$ species are quite similar. The oxidation/reduction procedures using O_2 and CO provide a very convenient method to reproducibly modify the Au/TiO_2 catalyst.

To determine the kinetic influence of oxidation of the Au/TiO_2 catalyst, we performed low-temperature CO oxidation reactions on the fully reduced catalyst and on the fully oxidized catalyst separately. Infrared spectra taken during the first 1200 s of the two experiments are shown in Figure 3. Consistent with our previous findings on Au^0/TiO_2 catalysts,[9] CO/TiO_2 is the main active species undergoing oxidation at 120 K judging by

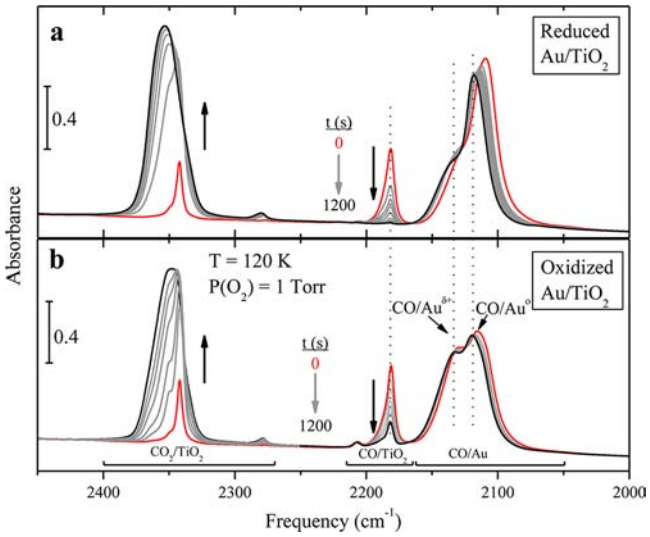

Figure 3. Comparison of low-temperature CO oxidation on the (a) fully reduced Au^0/TiO_2 catalyst and (b) fully oxidized $Au^{\delta+}/TiO_2$ catalyst.

the disappearance of the CO/TiO_2 feature from the IR spectra. An absorption band near 2350 cm^{-1}, corresponding to production of CO_2/TiO_2, is observed to increase. At 120 K, the CO_2 product is captured on the catalyst surface. The CO/Au^0 and $CO/Au^{\delta+}$ bands are slightly blue shifted during the reaction, indicating partial charge transfer by adsorbed oxygen atoms on nearby Au sites at 120 K. However, these CO/Au^0 and $CO/Au^{\delta+}$ species are not significantly consumed during the CO oxidation reaction due to their limited diffusional motion on Au sites at such low temperature.[9] This small blue shift disappears upon evacuation of O_2 and readsorption of CO at 120 K, as shown in Figure S4, Supporting Information. The main kinetic difference in the two experiments in Figure 3 is the decrease of the rate of CO/TiO_2 consumption (as well as CO_2/TiO_2 generation) on the fully oxidized $Au^{\delta+}/TiO_2$ catalyst. In 1200 s at 120 K, the CO/TiO_2 oxidation reaction is complete on the fully reduced Au^0/TiO_2 catalyst (Figure 3a), while ~20% of CO/TiO_2 remains on the $Au^{\delta+}/TiO_2$ catalyst (Figure 3b). Kinetic plots of the CO/TiO_2 consumption on fully reduced and fully oxidized Au/TiO_2 are shown in Figure 4, where a reversibility test for the catalyst during multiple reduction/oxidation cycles is also shown. The CO/TiO_2 oxidation reaction follows accurate first-order kinetics in CO coverage in both cases, indicated by the fitted solid lines in Figure 4. The catalyst performance is reproducible for the mild oxidation−reduction cycles used in this study. The first-order CO oxidation rate constant at 120 K is ~22 times larger on the fully reduced Au^0/TiO_2 catalyst compared to the $Au^{\delta+}/TiO_2$ catalyst, indicating an inhibition effect associated with formation of $Au^{\delta+}$ species. A similar reduction in the CO oxidation rate was also reported on a O_2-treated Au/SiO_2 catalyst working at room temperature.[49] It is noteworthy that the inhibition on $Au^{\delta+}/TiO_2$ is detected by the decrease of the rate of consumption of the CO/TiO_2 species, which is the only participant for CO oxidation at 120 K, showing again the unique activity of dual-catalyst sites at the Au perimeter for CO/TiO_2 oxidation on the Au/TiO_2 catalyst. As shown previously[9] and below, these sites involve Au and Ti centers which have a special capability to activate molecular O_2 at the perimeter of Au nanoparticles on TiO_2.

dx.doi.org/10.1021/ja304426b | J. Am. Chem. Soc. 2012, 134, 12717−12723

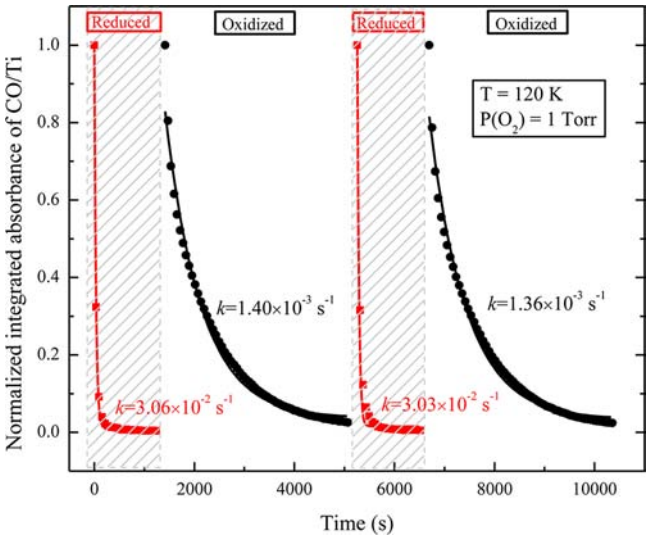

Figure 4. Representative kinetic plots of the CO/TiO_2 oxidation process on the fully reduced Au^0/TiO_2 catalyst (red, corresponding to Figure 3a) and fully oxidized $Au^{\delta+}/TiO_2$ catalyst (black, corresponding to Figure 3b). Solid lines represent the first-order kinetics fit for the experimental data.

Previously we reported the apparent activation energy for CO oxidation on the Au^0/TiO_2 catalyst to be 0.16 ± 0.01 eV.[9] For comparison we carried out a study of the effect of temperature on the CO/TiO_2 oxidation on the fully oxidized $Au^{\delta+}/TiO_2$ catalyst in the temperature range of 110−130 K as shown in Figure 5a. The resulting apparent activation energy

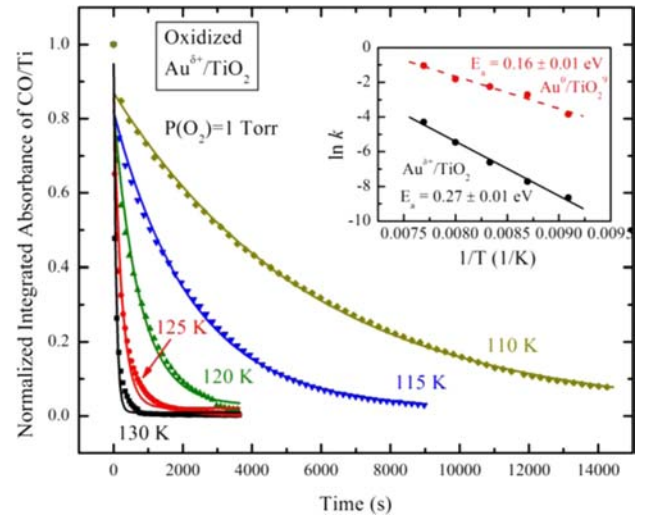

Figure 5. Plots of the integrated absorbance of CO/TiO_2 against time during reaction with O_2 at various temperatures fitted to first-order kinetics. (Inset) Arrhenius plot comparing activation energies on Au^0/TiO_2 (red) and $Au^{\delta+}/TiO_2$ (black). Data for Au^0/TiO_2 was taken from ref 9.

for oxidation of CO/TiO_2 was found to be 0.27 ± 0.01 eV (Figure 5b), a near doubling of apparent activation energy. The ratio of preexponential factors, $A_{ox}/A_{red} \approx 10^3$, indicates that the O inhibition of Au catalytic activity is likely not due to site blocking by adsorbed O atoms. We postulated previously that the lower activation energy process measured for CO oxidation over the Au^0/TiO_2 catalyst may be heavily influenced by the CO/TiO_2 species' diffusion energy across the TiO_2 surface.[9] The large difference in the pre-exponential factors therefore may indicate that the two Arrhenius plots are likely describing processes that differ in mechanism and activation entropy, where CO oxidation on $Au^{\delta+}$ sites is entropically more favorable. It is worth noting that working at low temperatures is important to see the reduction of catalytic activity associated with the presence of the $Au^{\delta+}$ site. At elevated temperatures near room temperature inhibition by chemisorbed oxygen will not be observed as the CO can migrate to the oxidized Au site and easily reduce it (Figure 2).

Density functional theory (DFT) calculations provided detailed insight into the mechanism for CO oxidation at the dual-catalytic sites of the Au^0/TiO_2 perimeter.[9] We carry out similar calculations herein to follow the influence of partially oxidized Au on the oxidation of CO at the dual Au/TiO_2 sites using the same Au/TiO_2 interface model presented previously.[9] A detailed charge analysis of the Au sites on the fully reduced Au/TiO_2 surface shows that all of the surface Au atoms are neutral, except for those that are in direct contact with the bridge oxygen atoms of the TiO_2 support which have a charge of ca. +0.1 e as shown in Figure S7, Supporting Information.

Some previous theoretical studies have suggested the importance of $Au^{\delta+}$ for CO oxidation on the Au/TiO_2 catalyst.[7,28−30,32] The models that were used examined only the influence of charge transfer between the TiO_2 support and the Au nanoparticles. There are no studies, however, of which we are aware that examine the influence of the preoxidation of Au nanoparticles by chemisorbed oxygen on Au/TiO_2 catalysts. These sites involving chemisorbed oxygen, however, are more likely to be the relevant sites associated with the inhibition phenomena that occur at O_2-rich conditions. We start by examining the Au sites where direct O_2 activation most likely proceeds. We showed previously that O_2 preferentially adsorbs at the perimeter sites along the Au/TiO_2 interface where it is partially activated by its interaction with the Au, thus forming a Ti−O−O−Au, peroxo-type intermediate.[9] Direct activation of O_2 at these perimeter sites, where no assistance by other molecules is involved, proceeds with a barrier of 0.4−0.6 eV (Figure S6, Supporting Information), resulting in production of O adatoms at the Au perimeter. Once formed, these O adatoms can diffuse to Au sites that are further removed from the perimeter as shown in Figure 6 (and Figure S8, Supporting Information). The favorable binding sites for these atomic O species is either on a FCC 3-fold hollow or on the edge bridge site, as shown in Figure S8a−c, Supporting Information. The binding energies for these chemisorbed O adatoms are from −0.3 to −0.4 eV with respect to one-half of the O_2 molecule in the gas phase, indicating that the O_2 dissociative adsorption is exothermic and chemisorbed O adatoms resulting from O_2 dissociation are stable. The higher activation barriers for O surface diffusion on Au are consistent with the fact that these sites form only at higher preoxidation temperatures (≥295 K). These O adatoms inductively increase the positive charge of the neighboring Au atoms as shown in Figure 6 ($Au^{\delta+}$, δ = 0.1−0.3) and directly influence the vibrational frequency of CO adsorbed on these electropositive Au sites. The vibrational frequency calculation results are reported in Figure 6. Calculated $CO/Au^{\delta+}$ frequencies reveal a blue shift of +14−23 cm^{-1} from CO/Au^0, which is in very good agreement with the +20 cm^{-1} shift observed experimentally (from ∼2106 to ∼2126 cm^{-1}, Figure 1).

dx.doi.org/10.1021/ja304426b | J. Am. Chem. Soc. 2012, 134, 12717−12723

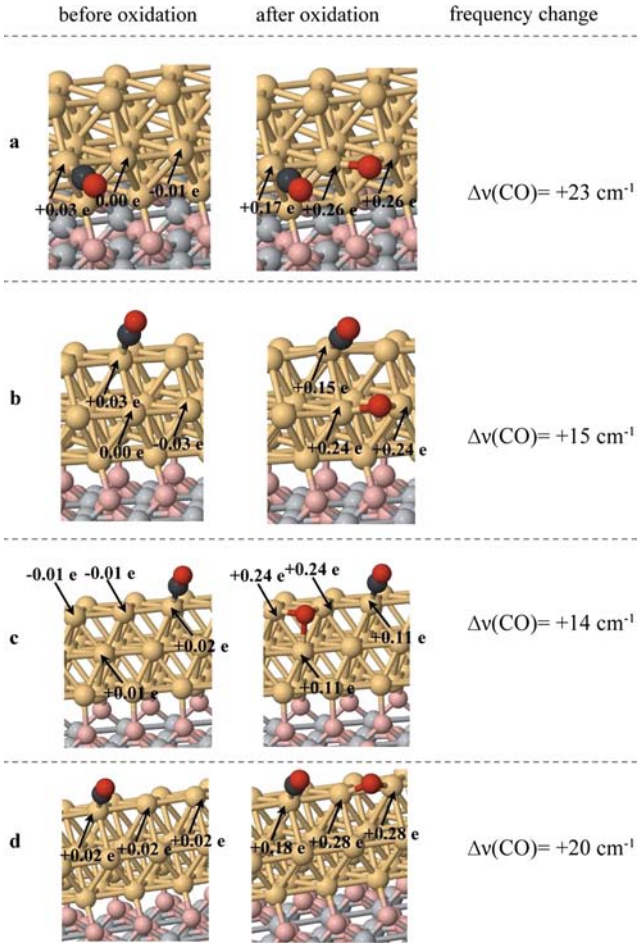

Figure 6. Theoretical predictions of the CO vibrational frequency change before and after oxidation. (a–d Different CO and O adsorption configurations on the Au nanorod.

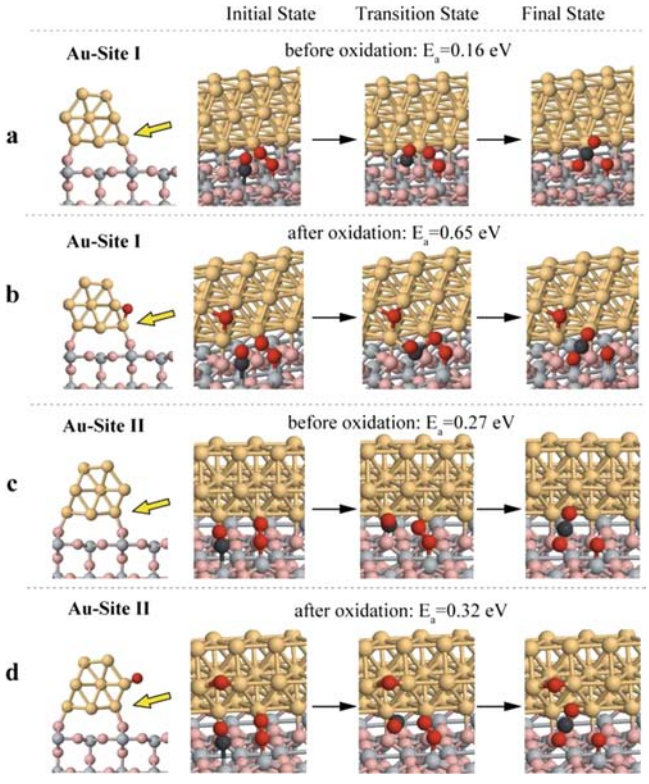

Figure 7. Oxygen inhibition effect for O–O bond scission at the Au/TiO_2 perimeter from DFT calculation. (a and b) CO-assisted O_2 dissociation at Au-Site I (a) before and (b) after Au oxidation by an O adatom. (c and d) CO-assisted O_2 dissociation at Au-Site II (a) before and (b) after Au oxidation by an O adatom.

CO oxidation at the Au^0/TiO_2 perimeter was found to follow a path where molecular O_2 is activated in the presence of a nearby CO molecule at a dual-catalytic site via a Au–O–O–Ti precursor.[9,23,28] We examine the two characteristically different perimeter sites present in our model as shown in Figure 7 (and in Figure S5, Supporting Information), which reveal the differences that result from the different coordination numbers (CN) of the Au atoms that bind to the TiO_2 support. The first site (site I, Figure 7a) involves a more coordinatively unsaturated Au atom (CN = 6) and is anchored to the support by a TiO_2-bridging oxygen atom. The second site (site II, Figure 7c) involves a Au atom with CN = 7 which also interacts with a TiO_2-bridging oxygen atom. The different coordination numbers at these sites provide insights into the behavior of Au atoms with different coordination numbers in contact with the TiO_2 support of actual catalysts. When the Au was not oxidized, the activation energies calculated for the O–O bond scission (assisted by CO at the perimeter) are 0.16 (site I) and 0.27 eV (site II), as shown in Figure 7a and 7c. The lower barrier for CO oxidation reported at site I is the result of the less-coordinatively saturated Au atom[50] in site I, strongly stabilizing the terminal O of O_2 on TiO_2. Similarly the higher barrier for CO oxidation at site II, compared to site I, is due to the weaker interaction of Au with O_2 that arises from the increased CN of the Au atom at site II over that at site I. In this case for the reduced Au^0/TiO_2 catalyst, CO oxidation can proceed at either site at 120 K, with site I being kinetically dominant. The presence of partially oxidized Au atoms that result upon formation of chemisorbed oxygen atoms reduces the ability of $Au^{\delta+}$ to stabilize the CO–O_2 formation in the transition state upon reaction with CO, thus increasing the activation barrier (Figure 7b and 7d). The CO oxidation activation barrier for $Au^{\delta+}$ at site I is now markedly higher at 0.65 eV as shown in Figure 7b. The activation barrier for site II shown in Figure 7d is only 0.32 eV. This significant activation barrier increase at site I is the result of the much stronger binding of the chemisorbed oxygen atom due to the lower CN of Au at site I (CN = 6) than at site II (CN = 7). The strong chemisorption of atomic oxygen at site I prohibits site I from carrying out catalytic oxidation, whereas site II can still catalyze CO oxidation at temperatures in the range 110–130 K. Since the preoxidation of the Au/TiO_2 catalyst was performed in 5 Torr of O_2 at elevated temperature (473 K), it is reasonable to assume the majority of perimeter sites are covered with O adatoms after oxidation. In fact, based on the changes in CO/Au and CO/$Au^{\delta+}$ absorbance in Figure 2, about 60% of the Au^0 sites on the surface of the Au nanoparticles become $Au^{\delta+}$ sites for the particular size distribution of the Au nanoparticles used in the experiment. As a result, Au–Site I is poisoned whereas Au–Site II becomes the most active site for CO oxidation at low temperatures. Reaction of CO with the first oxygen of O_2 at Au–Site II results in formation of CO_2 and an O adatom on the TiO_2 perimeter. This bound oxygen atom reacts with a second CO molecule on the TiO_2 support to form CO_2 with a barrier of only ~0.1 eV to regenerate the active site.

dx.doi.org/10.1021/ja304426b | J. Am. Chem. Soc. 2012, 134, 12717–12723

The end result from the theoretical simulations is that formation of strongly chemisorbed oxygen bound to coordinatively unsaturated Au atoms inhibits these sites for low-temperature CO oxidation. The more coordinatively saturated Au atoms associated with bound oxygen atoms can still oxidize CO, but the barrier is increased to 0.32 eV, which is consistent with the experimentally observed inhibition of the Au/TiO_2 catalyst by preoxidation and agrees with the 0.27 eV measured apparent activation energy.

Preoxidation is carried out in a temperature range where Au-based catalytic reactions are usually performed (295−473 K). At these temperatures, $Au^{\delta+}$ species formed from oxygen chemisorption are likely to be involved. The apparent activation energy of 0.27 eV on the $Au^{\delta+}/TiO_2$ catalyst agrees with previously reported 0.2−0.3 eV activation energies for CO oxidation on Au/TiO_2 catalysts measured at higher temperatures (200−350 K).[51,52] While these partially oxidized sites demonstrate reactivity that is consistent with that reported over working catalysts, the higher temperature used here to activate O_2 also promotes diffusion of adsorbed atomic oxygen from the interface where it can react with CO on Au^0 sites. In our low-temperature experiments, the more active Au^0 metal sites at the Au perimeter are only present at temperatures below 200 K. This argument is confirmed by extension of the Arrhenius plots shown in Figure 5b, where CO oxidation activity on the $Au^{\delta+}$ sites surpasses the Au^0 sites at 198 K. In the temperature range of $T > 198$ K, CO reacts with the O adatoms on the Au nanorod, constantly reducing the $Au^{\delta+}$ sites to Au^0 sites, and the activity increases above that observed when $Au^{\delta+}$ sites remain unreduced, below 147 K (Figure 2). The $Au^{\delta+}$ sites exhibit lower reactivity than Au^0 sites, which is consistent with the results from in situ X-ray absorption studies of CO oxidation over Au/TiO_2 catalysts at higher temperatures.[3,18,19,53,54]

IV. CONCLUSION

The activity of Au catalytic sites located at the boundary between Au nanoparticles and a TiO_2 support has been studied experimentally and theoretically in order to understand the influence of oxygen adsorption on the model low-temperature oxidation reaction, $CO + 1/2O_2 \rightarrow CO_2$. As on the reduced Au/TiO_2 catalyst, CO is found to be supplied from TiO_2 sites surrounding the preoxidized Au nanoparticles at catalytic reaction temperatures near 120 K, confirming the general picture of catalytic activity at the nanoparticle perimeter. It is found that on the oxygen-treated catalyst the reaction rate is considerably reduced and the activation energy is nearly doubled by electronic effects which involve induction of positive charge into the perimeter Au atoms by O atom adsorption. Aactivation of O_2 on the inhibited $Au^{\delta+}$ catalyst is assisted by a neighboring CO molecule at low temperatures. The ability of the catalyst to activate molecular O_2 at dual-perimeter sites involving $Au^{\delta+}$ atoms and neighbor Ti^{4+} ions in the support is retarded significantly for the CN = 6 $Au^{\delta+}$ atoms, causing the catalytic site to shift to the CN = 7 $Au^{\delta+}$ sites. It is likely that the higher temperature and higher O_2 pressure regimes for CO oxidation involve these $Au^{\delta+}$ perimeter sites, where oxidation of Au^0 to $Au^{\delta+}$ by O_2 and reduction of $Au^{\delta+}$ to Au^0 by CO occur constantly.

■ ASSOCIATED CONTENT

Supporting Information

Detailed description of the experimental procedure and calculation parameters as well as extra calculation results. This material is available free of charge via the Internet at http://pubs.acs.org.

■ AUTHOR INFORMATION

Corresponding Author

E-mail: johnt@virginia.edu

Notes

The authors declare no competing financial interest.

■ ACKNOWLEDGMENTS

We gratefully acknowledge the financial support by DOE, Office of Basic Energy Sciences, under grant number DE-FG02-09ER16080 as well as a fellowship for Mrs. Isabel Green from AES Corp. through the AES Graduate Fellowships in Energy Research Program at the University of Virginia. We also acknowledge the XSEDE computing resources from the Texas Advanced Computing Center.

■ REFERENCES

(1) Haruta, M.; Kobayashi, T.; Sano, H.; Yamada, N. *Chem. Lett.* **1987**, *2*, 405−408.
(2) Meyer, R.; Lemire, C.; Shaikhutdinov, S. K.; Freund, H.-J. *Gold Bull.* **2004**, *37*, 72−124.
(3) Kung, M. C.; Davis, R. J.; Kung, H. H. *J. Phys. Chem. C* **2007**, *111*, 11767−11775.
(4) Widmann, D.; Behm, R. J. *Angew. Chem., Int. Ed.* **2011**, *50*, 10241−10245.
(5) Chen, M. S.; Goodman, D. W. *Science* **2004**, *306*, 252−255.
(6) Kotobuki, M.; Leppelt, R.; Hansgen, D. A.; Widmann, D.; Behm, R. J. *J. Catal.* **2009**, *264*, 67−76.
(7) Laursen, S.; Linic, S. *J. Phys. Chem. C* **2009**, *113*, 6689−6693.
(8) Wang, J.; Hammer, B. *Top. Catal.* **2007**, *44*, 49−56.
(9) Green, I. X.; Tang, W.; Neurock, M.; Yates, J. T., Jr. *Science* **2011**, *333*, 736−739.
(10) Green, I. X.; Tang, W.; Neurock, M.; Yates, J. T., Jr. *Angew. Chem., Int. Ed.* **2011**, *50*, 10186−10189.
(11) Yan, Z.; Chinta, S.; Mohamed, A. A.; Fackler, J. P.; Goodman, D. W. *J. Am. Chem. Soc.* **2005**, *127*, 1604−1605.
(12) Sanchez, A.; Abbet, S.; Heiz, U.; Schneider, W. D.; Häkkinen, H.; Barnett, R. N.; Landman, U. *J. Phys. Chem. A* **1999**, *103*, 9573−9578.
(13) Vijay, A.; Mills, G.; Metiu, H. *J. Chem. Phys.* **2003**, *118*, 6536−6551.
(14) Fu, Q.; Saltsburg, H.; Flytzani-Stephanopoulos, M. *Science* **2003**, *301*, 935−938.
(15) Fierro-Gonzalez, J. C.; Guzman, J.; Gates, B. C. *Top. Catal.* **2007**, *44*, 103−114.
(16) Frondelius, P.; Häkkinen, H.; Honkala, K. *Angew. Chem., Int. Ed.* **2010**, *49*, 7913−7916.
(17) Venezia, A. M.; Pantaleo, G.; Longo, A.; Di Carlo, G.; Casaletto, M. P.; Liotta, F. L.; Deganello, G. *J. Phys. Chem. B* **2005**, *109*, 2821−2827.
(18) Calla, J. T.; Bore, M. T.; Datye, A. K.; Davis, R. J. *J. Catal.* **2006**, *238*, 458−467.
(19) Calla, J.; Davis, R. *Catal. Lett.* **2005**, *99*, 21−26.
(20) Laursen, S.; Linic, S. *Phys. Rev. Lett.* **2006**, *97*, 026101−1−4.
(21) Molina, L. M.; Hammer, B. *Appl. Catal., A* **2005**, *291*, 21−31.
(22) Vilhelmsen, L. B.; Hammer, B. *Phys. Rev. Lett.* **2012**, *108*, 126101−1−5.
(23) Liu, Z.-P.; Hu, P.; Alavi, A. *J. Am. Chem. Soc.* **2002**, *124*, 14770−14779.

(24) Okazaki, K.; Morikawa, Y.; Tanaka, S.; Tanaka, K.; Kohyama, M. *Phys. Rev. B* **2004**, *69*, 235404−1−8.
(25) Madsen, G. K. H.; Hammer, B. *J. Chem. Phys.* **2009**, *130*, 044704−1−7.
(26) Okumura, M.; Kitagawa, Y.; Haruta, M.; Yamaguchi, K. *Appl. Catal., A* **2005**, *291*, 37−44.
(27) Okumura, M.; Kitagawa, Y.; Haruta, M.; Yamaguchi, K. *Chem. Phys. Lett.* **2001**, *346*, 163−168.
(28) Molina, L. M.; Rasmussen, M. D.; Hammer, B. *J. Chem. Phys.* **2004**, *120*, 7673−7680.
(29) Wang, J. G.; Hammer, B. *Phys. Rev. Lett.* **2006**, *97*, 136107−1−4.
(30) Liu, Z.-P.; Gong, X.-Q.; Kohanoff, J.; Sanchez, C.; Hu, P. *Phys. Rev. Lett.* **2003**, *91*, 266102−1−4.
(31) Boronat, M.; Concepción, P.; Corma, A. *J. Phys. Chem. C* **2009**, *113*, 16772−16784.
(32) Chrétien, S.; Metiu, H. *J. Chem. Phys.* **2008**, *128*, 044714−1−13.
(33) Remediakis, I. N.; Lopez, N.; Nørskov, J. K. *Appl. Catal., A* **2005**, *291*, 13−20.
(34) Tang, D.; Hu, C. *J. Phys. Chem. Lett.* **2011**, 2972−2977.
(35) Laursen, S.; Linic, S. *Phys. Chem. Chem. Phys.* **2009**, *11*, 11006−11012.
(36) van Bokhoven, J. A.; Louis, C.; Miller, J. T.; Tromp, M.; Safonova, O. V.; Glatzel, P. *Angew. Chem., Int. Ed.* **2006**, *45*, 4651−4654.
(37) Li, M.; Wu, Z.; Ma, Z.; Schwartz, V.; Mullins, D. R.; Dai, S.; Overbury, S. H. *J. Catal.* **2009**, *266*, 98−105.
(38) Minicò, S.; Scirè, S.; Crisafulli, C.; Visco, A. M.; Galvagno, S. *Catal. Lett.* **1997**, *47*, 273−276.
(39) Dekkers, M. A. P.; Lippits, M. J.; Nieuwenhuys, B. E. *Catal. Lett.* **1998**, *56*, 195−197.
(40) Zanella, R.; Giorgio, S.; Henry, C. R.; Louis, C. *J. Phys. Chem. B* **2002**, *106*, 7634−7642.
(41) Lee, I.; Joo, J. B.; Yin, Y.; Zaera, F. *Angew. Chem., Int. Ed.* **2011**, *50*, 10208−10211.
(42) Perdew, J. P.; Wang, Y. *Phys. Rev. B* **1992**, *45*, 13244−13249.
(43) Henao, J. D.; Caputo, T.; Yang, J. H.; Kung, M. C.; Kung, H. H. *J. Phys. Chem. B* **2006**, *110*, 8689−8700.
(44) Carrettin, S.; Concepción, P.; Corma, A.; López Nieto, J. M.; Puntes, V. F. *Angew. Chem., Int. Ed.* **2004**, *43*, 2538−2540.
(45) Chen, M.; Goodman, D. W. *Acc. Chem. Res.* **2006**, *39*, 739−746.
(46) Hao, Y.; Mihaylov, M.; Ivanova, E.; Hadjiivanov, K.; Knözinger, H.; Gates, B. C. *J. Catal.* **2009**, *261*, 137−149.
(47) Mihaylov, M.; Knözinger, H.; Hadjiivanov, K.; Gates, B. C. *Chem. Ing. Tech.* **2007**, *79*, 795−806.
(48) Boccuzzi, F.; Chiorino, A.; Manzoli, M. *Surf. Sci.* **2000**, *454*−*456*, 942−946.
(49) Wu, Z.; Zhou, S.; Zhu, H.; Dai, S.; Overbury, S. H. *J. Phys. Chem. C* **2009**, *113*, 3726−3734.
(50) Williams, W. D.; Shekhar, M.; Lee, W. S.; Kispersky, V.; Delgass, W. N.; Ribeiro, F. H.; Kim, S. M.; Stach, E. A.; Miller, J. T.; Allard, L. F. *J. Am. Chem. Soc.* **2010**, *132*, 14018−14020.
(51) Daté, M.; Okumura, M.; Tsubota, S.; Haruta, M. *Angew. Chem., Int. Ed.* **2004**, *43*, 2129−2132.
(52) Long, C. G.; Gilbertson, J. D.; Vijayaraghavan, G.; Stevenson, K. J.; Pursell, C. J.; Chandler, B. D. *J. Am. Chem. Soc.* **2008**, *130*, 10103−10115.
(53) Weiher, N.; Bus, E.; Delannoy, L.; Louis, C.; Ramaker, D. E.; Miller, J. T.; van Bokhoven, J. A. *J. Catal.* **2006**, *240*, 100−107.
(54) Schwartz, V.; Mullins, D. R.; Yan, W.; Chen, B.; Dai, S.; Overbury, S. H. *J. Phys. Chem. B* **2004**, *108*, 15782−15790.